

Ultraviolet-infrared double-resonance laser spectroscopy of nd ($n = 12-17$) Rydberg states in ^3He

L. A. Bloomfield, H. Gerhardt, and T. W. Hänsch

Department of Physics, Stanford University, Stanford, California 94305

(Received 24 September 1982)

The hyperfine structure of the singlet and triplet nd Rydberg states ($n = 12-17$) in ^3He have been studied by Doppler-free ultraviolet-infrared double-resonance laser spectroscopy. Using the frequency-doubled output of a cw dye ring laser we have populated the $1s5p\ ^3P$ state of ^3He by excitation from the metastable $1s2s\ ^3S$ state at 294.5 nm. In a second step, an infrared single-mode cw color center laser is used to excite d Rydberg states. The experimental results for the $n\ ^1,^3D$ hyperfine splittings ($n = 12-17$) are in excellent agreement with semiempirical calculations using hydrogenlike wave functions. Anomalous isotopic shifts in the electrostatic energy intervals of 5 to 20 MHz were found for the states $n = 12-17$. These shifts are smaller than the shifts of about 35 MHz found for the states $n = 5-8$ with the help of anticrossing spectroscopy. No satisfactory explanation of these shifts has yet been found.

I. INTRODUCTION

The helium atom is the simplest multielectron system and is therefore ideally suited for the study of electron-electron interactions. In ^3He Rydberg states, perturbations due to singlet-triplet induced fine and hyperfine (hf) mixing play an important role, however, no previous measurements in states with principal quantum numbers $n > 8$ exist. Singlet-triplet splittings of $n\ ^1D-n\ ^3D$ ($n = 3-8$) were measured by anticrossing spectroscopy.^{1,2} Results on the hf splittings of $n\ ^1D$ states ($n = 3-7$) were obtained by level crossing spectroscopy.³ The hf splittings in the $n\ ^3S$ and $n\ ^3D$ states ($n = 3-6$) were investigated by Doppler-free two-photon spectroscopy with cw dye lasers.⁴ Two-photon transitions to levels with principal quantum numbers higher than $n = 6$ require cw laser radiation in the coumarin-dye wavelength range. The low output power of the inefficient coumarin lasers makes two-photon spectroscopy in these states difficult.

The availability of efficient frequency-doubled cw dye lasers has made it possible to study high-lying Rydberg states in ^3He by double-resonance spectroscopy. Using a single-mode cw dye ring laser to pump an external frequency doubler inside a passive enhancement cavity, we have populated the $1s5p\ ^3P$ state of ^3He by excitation from the metastable $1s2s\ ^3S$ state at 294.5 nm. In a second step, an infrared single-mode cw color center laser is used to excite d Rydberg states with $n \geq 12$. With the laser beams oriented parallel or antiparallel, the experiment yields spectra free of Doppler broadening.⁵ In this paper, we report on double-resonance spectroscopy

of the $n\ ^1D$ and $n\ ^3D$ Rydberg states ($n = 12-17$) of ^3He . We obtained results on the singlet and triplet hf splittings as well as the singlet-triplet electrostatic energy intervals. We compare our results with semiempirical calculations and with the results obtained in nd states ($n = 5-8$) by anticrossing spectroscopy.^{1,2}

In Sec. II, experimental details will be given. Section III discusses the principles of the semiempirical calculations. The experimental results are given in Sec. IV, along with a discussion and a comparison with other experiments.

II. EXPERIMENTAL APPARATUS

A scheme of the experimental setup is shown in Fig. 1. Metastable helium atoms are produced by bombarding high-purity ^3He gas of 25 mTorr inside a chamber with electrons of 50-eV energy from an electron gun. The gas pressure is significantly lower than that required for a dc discharge. The electron gun consists of a flat dispenser cathode, 3 mm in diameter, and is indirectly heated by a bifilar heater. The electron beam is extracted through two grids: a control grid and a ground potential grid. The cathode is biased at a negative potential with respect to ground. Transmitted electrons are collected by a flat plate anode. At 50-eV potential, an electron current of 10 mA emerges from the gun. Although no magnetic field is applied, a well-collimated beam is achieved. For pulsed operation and gated detection, negative voltage pulses are applied to the control grid.

The color center laser and the uv laser beams

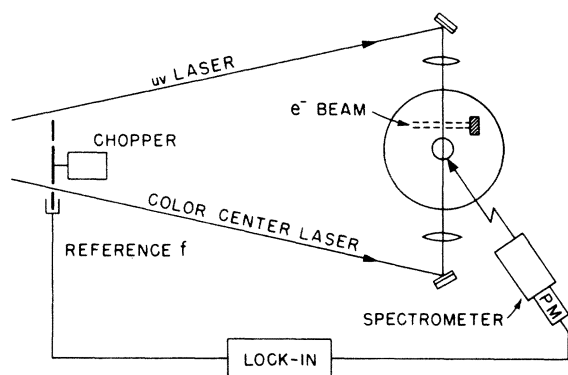


FIG. 1. Schematic diagram of the experimental apparatus.

counterpropagate through the helium chamber. The infrared radiation is chopped at a frequency $f_m = 1440$ Hz. The interaction region is kept at a distance of 25 mm from the electron beam so that only thermally diffused metastable atoms are present, and electric fields due to the electron beam are kept to a minimum. The double-resonance signal is recorded by observing a modulation at frequency f_m in the intensity of the fluorescence at the uv excitation wavelength. The fluorescent light is collected in a direction perpendicular to the laser beams by a lens of 10-cm focal length and is focused on the entrance slit of a 25-cm monochromator. The output signal of an Amperex 56AVP photomultiplier is fed into a lock-in amplifier.

The beams are focused to 0.5 mm diameter in the interaction region. The polarizations of the beams are linear and parallel to one another. The spectra obtained are Doppler-free because the uv laser selectively interacts, within the homogeneous width, with atoms Doppler shifted into resonance, and only these atoms are available for the excitation by the infrared laser. With a choice of counterpropagating beams, the resonances are further narrowed by coherence effects.⁶

The ultraviolet radiation is produced by second harmonic generation in a passive ring enhancement cavity, pumped with 1.4 W of 589.0-nm radiation from a Coherent 699-21 ring dye laser.⁷ The cavity has the same configuration as the dye laser. A 23-mm ammonium dihydrogen arsenate crystal with Brewster surfaces is placed in one of the beam waists, and the generated uv radiation exits the cavity through a dichroic fold mirror. We employ 90° phase matching and the crystal temperature is stabilized to within 0.03°C.

The enhancement cavity has an enhancement of 20 and is locked on resonance by analyzing the reflected light from the input mirror.⁸ A dispersion-shaped error signal is generated from the difference

current of two photodiodes, and this signal is integrated and amplified to yield a unipolar high voltage. The 0–1-kV output controls a piezoelectric translator. With this translator the cavity will track the laser input frequency for up to 1.4 GHz before the piezo drive saturates at high voltage. In order to allow for large frequency scans and to avoid unlocking on high-voltage saturation, an active rellocking scheme was implemented. This additional circuitry senses imminent lock failure and forces the cavity to jump to the next mode. In our experiment, the effect of rellocking on the signal is negligible due to the lock-in time constant of a second or more.

In order to maintain stable dye laser pump power at a level of 1.4-W single mode, we have enclosed the ring laser in a plastic, dustfree chamber and refrigerate the ethylene glycol based rhodamine 6G dye solution. This eliminates temperature fluctuations as well as contamination and permits continuous operation at the highest available power over many hours. Our peak uv power is over 50 mW, and we normally operate between 35 and 45 mW.

The infrared color center laser, a modified Burleigh FCL-20, was pumped with the output of a multimode cw dye laser. All lines from a Spectra-Physics 165 argon ion laser (4.5 W) were used to pump a Spectra-Physics 375 dye laser. Operated with rhodamine 6G dye and without internal cavity etalons, an output power of 900 mW was emitted. The dye laser wavelength was tuned to optimize the output power of the FCL-20. The wavelength range 2.4–2.52 μm was covered using a KCl:Na crystal, giving an output power of approximately 6 mW. The transitions $5p$ to nd ($n = 15$ –17) can be accessed using this crystal. For the range 2.52–2.7 μm , a KCl:Li crystal was employed with an output power of 10 mW. In this case, the levels $n = 12$ –14 could be measured. A reliable, continuously tunable single-mode output from the color center laser was achieved only after the insertion of an additional etalon into the cavity. This solid etalon has a thickness of 3 mm.

Figure 2 is an example of a spectrum, showing a Doppler-free double-resonance scan of the 2^3S - 5^3P - $13^1,3D$ transition in ^3He with all strong hf components. For this scan, the single-mode uv laser was positioned at the center of the absorption profile of the 2^3S - 5^3P transition by actively locking to a stabilized Fabry-Perot resonator. The color center laser was scanned across the hf components of the 5^3P - $13^1,3D$ line. Frequency measurements were accomplished using a confocal infrared interferometer with a free spectral range of 149.82 ± 0.05 MHz. The measured hf intervals were corrected for frequency shifts due to different intervals in the hf levels of the 5^3P state. For the $5p$ - nd transitions, reso-

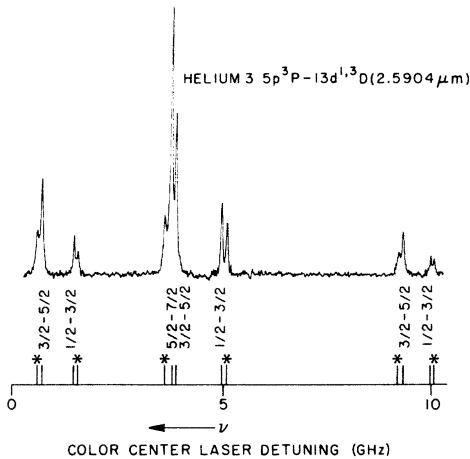


FIG. 2. Doppler-free double-resonance scan of the 2^3S - 5^3P - $13^{1,3}D$ transition in ^3He . Lines marked by a star are collisionally induced hf transition peaks.

nances are observed at

$$\Omega_{\text{ir}} = \omega_{\text{ir}} - \frac{\omega_{\text{ir}}}{\omega_{\text{uv}}} (\Omega_{\text{uv}} - \omega_{\text{uv}}), \quad (1)$$

where ω_{uv} is the frequency of the $2s$ - $5p$ transition, ω_{ir} is the frequency of the $5p$ - nd transition, and Ω_{uv} is the frequency of the fixed uv laser.

The observed linewidth (full width at half maximum) of 35 MHz is larger than the natural linewidth of about 1 MHz as given by the natural lifetime of the 5^3P state. The main broadening mechanism is pressure broadening. Electric fields have no influence on the linewidths or hf splittings, as we have shown using pulsing and gated techniques.

III. THEORY

The strong interaction of the unpaired $1s$ electron with the ^3He nucleus and the hf induced singlet-triplet mixing significantly modify the hf splittings of the nd states. Because J is not a good quantum number, we have calculated the eigenvalues and relative intensities for the nd subspaces in an uncoupled representation. The Hamiltonian for the nd subspace is given by

$$H = H_0 + H_{\text{fs}} + H_{\text{hfs}}, \quad (2)$$

where H_0 determines the energy of the spinless electron. We assume H_0 to be diagonal in the uncoupled basis. The fine-structure Hamiltonian for a two-electron atom in parametrized form is given by⁹

$$H_{\text{fs}} = A \vec{L} \cdot \vec{S} + a \vec{L} \cdot \vec{K} + b \left[\frac{3(\vec{L} \cdot \vec{S})^2 + \frac{3}{2} \vec{L} \cdot \vec{S} - \vec{L}^2 \cdot \vec{S}^2}{2S(2S-1)L(2L-1)} \right], \quad (3)$$

where $\vec{L} = \vec{l}_1 + \vec{l}_2$, $\vec{S} = \vec{s}_1 + \vec{s}_2$, $\vec{K} = \vec{s}_1 - \vec{s}_2$, and A , a , and b are the spin-orbit, the spin-orbit singlet-triplet, and the spin-spin coupling constants, respectively. For the hf Hamiltonian of the d states, the parameterized form is given by

$$H_{\text{hfs}} = C \vec{I} \cdot \vec{S} + C \vec{I} \cdot \vec{K}, \quad (4)$$

where the constant C describes the Fermi contact interaction. In d Rydberg states, nuclear-spin electron-spin-orbit interactions can be neglected. Singlet-triplet mixing is given only by the antisymmetric $\vec{L} \cdot \vec{K}$ and $\vec{I} \cdot \vec{K}$ terms. The contribution of the Fermi contact term results from the spin density of the $1s$ electron at the nucleus. Therefore, both terms in Eq. (4) have the same coupling constant and are independent of the quantum number n of the excited electron. Since the electrostatic energy separations decrease with increasing n , perturbations due to singlet-triplet mixing become more effective at higher n levels.

Calculations of the hf splittings of the 1D levels of ^3He were carried out by Bessis *et al.*¹⁰ using the hydrogenic approximation for the states $n=3-8$. In this approximation, the wave functions are linear combinations of Slater determinants built on the single configuration $(1s, nd)$, where $1s$ and nd are hydrogenlike functions. We adopted this method for the determination of the fine and hf constants of higher d states.

The hydrogenic constants calculated for the nd states ($n=12-17$) are listed in Table I. The theoretical Fermi contact term C_{theor} is derived from Ref. 11. Eigenvalues were obtained by diagonalizing the complete Hamiltonian matrix for the nd subspaces with the calculated hydrogenic constants and the experimentally determined electrostatic energy intervals

$$E_0(^4\text{He}) = E(^1D) - E(^3D)$$

(see Table IV). In Table II, first column, we list as an example the eigenvalues calculated for the $13d$ subspace. For comparison, the energy values of the $13d$ state in ^4He are listed in column 3, as calculated by omitting the hf interaction from the Hamiltonian. The influence of singlet-triplet mixing in ^3He is clearly seen. For instance, the two singlet levels are shifted about 7 GHz to higher frequencies. The classification of the $13d$ level of ^3He into singlet and triplet states is thus artificial and only used to identify the different hf components. In ^4He , singlet-triplet mixing alters the value of the electrostatic fine-structure interval by only 60 KHz. Therefore, the uncorrected E_0 value can be used.

With the eigenvector matrices calculated for the 5^3P and d states, we have computed intensities of the

TABLE I. Calculated and experimentally determined fine and hf structure constants for nd states ($n = 12-17$) in ${}^3\text{He}$. The theoretical constants are obtained by use of hydrogenlike wave functions (Refs. 10 and 11). The constants A_{expt} and b_{expt} are derived from Ref. 13. C_{expt} is given by the ground-state splitting of the ${}^3\text{He}^+$ ion (Ref. 14). Numbers are given in MHz.

State	A_{theor}	b_{theor}	C_{theor}	a_{theor}	A_{expt}	b_{expt}	C_{expt}
12 <i>d</i>	-3.4	7.7	4332.8	-10.1	-3.4	7.8	4332.8
13 <i>d</i>	-2.7	6.1	4332.8	-8.0	-2.7	6.1	4332.8
14 <i>d</i>	-2.2	4.9	4332.8	-6.4	-2.2	4.9	4332.8
15 <i>d</i>	-1.7	4.0	4332.8	-5.2	-1.8	4.0	4332.8
16 <i>d</i>	-1.4	3.3	4332.8	-4.3	-1.4	3.3	4332.8
17 <i>d</i>	-1.2	2.7	4332.8	-3.6	-1.2	2.7	4332.8

hf transitions. The intensities are concentrated in a few components due to the strong mixing, a fact which greatly simplifies the spectrum. The components appearing in Fig. 1 are the only transitions predicted to have significant intensity and differ from calculated transition probabilities by at most a few percent. In Table III, the computed intensities for the strong hf components of the $5^3P-13^{1,3}D$ transition are listed. Virtually identical intensities are calculated for transitions to other d Rydberg states.

IV. RESULTS AND DISCUSSION

The assignment of the spectrum in Fig. 2 is possible with the help of the calculated eigenvalues for the $13d$ state and the hf splittings of the 5^3P state.⁷ These splittings were measured to an accuracy of 1 MHz by intermodulated fluorescence spectroscopy with the same uv laser used in the present experiments. In the level diagram (Fig. 3) of the 5^3P and the $13^{1,3}D$ states, we have indicated the transitions corresponding to observed components. Besides the

triplet components, we have observed two strong components of the intercombination line. The hf intervals in the spectrum are given by the sum or difference of splittings of the $13d$ and 5^3P states. These intervals vary from a hundred MHz to several GHz. Thus, despite an experimental linewidth of about 35 MHz, it is possible to obtain results on d -state splittings of a few MHz. In the second column of Table II, we list the energies of the 13^1D and 13^3D levels, measured with respect to the $(3) \frac{7}{2}$ hf component. The calculated and measured hf splittings in the 1D and 3D subspaces agree within the experimental uncertainty of at most 4 MHz.

The agreement found between calculated and measured hf splittings in 1D and 3D subspaces is well within the experimental error, indicating that the use of hydrogenic wave functions is sufficiently precise at an uncertainty level of a few MHz. Investigations of the n^3D ($n = 3-6$) states by intermodulated fluorescence spectroscopy and two-photon spectroscopy^{4,12} have also shown good agreement with calculated hf structure. For the fine and hf

TABLE II. Energy values for the hf components of the $13d$ level in ${}^3\text{He}$ and ${}^4\text{He}$. The zero value corresponds to the 13^3D level in the absence of fine and hf contributions. The ${}^4\text{He}$ results are obtained from Ref. 13. Numbers are given in MHz.

	${}^3\text{He}$				${}^4\text{He}$	
	J	F	Theory	Experiment	J	Fitted results
13^1D	2	$\frac{5}{2}$	7199.2	7196.7 ± 4.0	2	2269.0
	2	$\frac{3}{2}$	7182.6	7180.7 ± 4.0		
13^3D	1	$\frac{3}{2}$	-575.4	-578.6 ± 4.0	1	13.4
	2	$\frac{5}{2}$	-600.8	-602.6 ± 4.0	2	-2.7
	1	$\frac{1}{2}$	-2153.0	-2155.6 ± 3.0	3	-3.9
	2	$\frac{3}{2}$	-2161.0	-2163.6 ± 3.0		
	3	$\frac{5}{2}$	-2169.4	-2168.2 ± 3.0		
	3	$\frac{7}{2}$	-2170.3	-2170.3		

TABLE III. Normalized intensities of the strong components for the 5^3P - $13^{1,3}D$ transition in ^3He .

		5^3P				
		(0) $\frac{1}{2}$	(1) $\frac{3}{2}$	(1) $\frac{1}{2}$	(2) $\frac{5}{2}$	(2) $\frac{3}{2}$
13^1D	(2) $\frac{5}{2}$		47.9			
	(2) $\frac{3}{2}$	25.2	5.2			
13^3D	(2) $\frac{5}{2}$		27.5			
	(1) $\frac{3}{2}$	15.0	2.9			
	(1) $\frac{1}{2}$			20.6		4.2
	(2) $\frac{3}{2}$			20.4	2.3	26.5
	(3) $\frac{5}{2}$				21.9	52.3
	(3) $\frac{7}{2}$				100.0	

constants, either hydrogenic or experimentally determined values have been used.

Values for the electrostatic energy separation E_0 in d states of the ^3He atom can be derived from the measured hf splittings if we assume that the hydrogenic constants listed in Table I are correct. As can be seen in Table I, the calculated fine-structure constants A and b , and the Fermi contact term C agree within a hundred kHz of experimentally determined values.^{13,14} The Fermi contact term C_{expt} is obtained from the measured ground-state splitting of the $^3\text{He}^+$ ion. It is assumed that the nd electron has no contribution to the spin density at the nucleus. For the spin-orbit singlet-triplet coupling constant a ,

no experimental values exist, and we are entirely dependent on the theoretical values. However, the good agreement between hydrogenic constants and experimentally determined constants and the measured and calculated hf splittings in 1D and 3D subspaces is a strong indication that the use of a_{theor} values is sufficiently precise.

In Table IV, first column, we list the electrostatic energy intervals E_0 for $n=12-17$ as determined from the measured hf splittings. Different $E_0(^3\text{He})$ values result in a change of the splittings between the (3) $\frac{7}{2}$ level and the levels (2) $\frac{5}{2}$, (1) $\frac{3}{2}$, (2) $\frac{3}{2}$, and (2) $\frac{5}{2}$. The listed electrostatic energy intervals are averages obtained from these measured splittings. The uncertainty intervals reflect the signal-to-noise ratio and the resolution achieved for the different nd states. In addition, we have listed the $E_0(^3\text{He})$ values for the nd ($n=5-8$) states, measured by anticrossing spectroscopy.^{1,2} The anticrossing measurements provided results only on the electrostatic intervals so that other results cannot be compared. The E_0 intervals for the $n=3,4$ states are not known as accurately, so that we have not considered these states. For comparison, we have listed the best-known $E_0(^4\text{He})$ in column 2. In column 3, we give the difference

$$\Delta E_0 = E_0(^4\text{He}) - E_0(^3\text{He}).$$

In Fig. 4, we have plotted $\Delta E_0(nd)$ values as a function of the principal quantum number n . For the states $n=12-17$, the $E_0(^3\text{He})$ values are measured to be 5–20 MHz less than the $E_0(^4\text{He})$ values. A systematic difference of about 35 MHz was measured for the states $n=5-8$.^{1,2} No clear connection is seen between the two groups of measurements. The large isotopic shifts measured for the $n(^1D-^3D)$ intervals are surprising because mass-dependent iso-

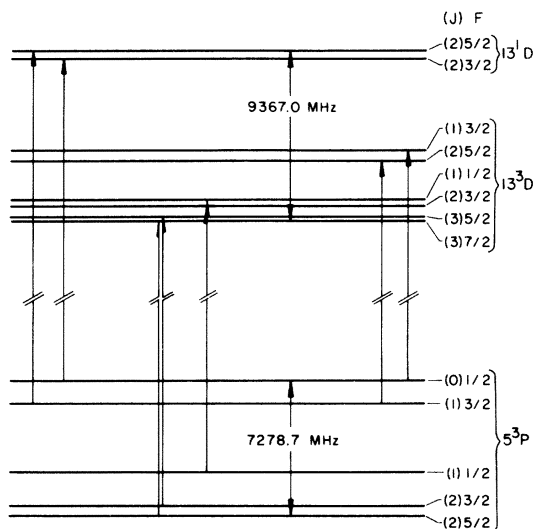


FIG. 3. Level diagram (not to scale) of the 5^3P and $13^{1,3}D$ states in ^3He . The transitions corresponding to observed components in the spectrum of Fig. 2 are indicated.

TABLE IV. Electrostatic energy intervals E_0 in ^3He and ^4He for nd states ($n=5-8$ and $n=12-17$). Column 3 gives the difference between ^4He and ^3He E_0 values. Numbers are given in MHz.

Level	$E_0(^3\text{He})$	$E_0(^4\text{He})$	$\Delta E_0(^4\text{He}-^3\text{He})$
5d	34 026 \pm 15 ^a	34 066.3 \pm 7.2 ^b	40.3 \pm 15
6d	20 885 \pm 5 ^c	20 919.2 \pm 1.5 ^d	34.2 \pm 5
7d	13 601 \pm 5 ^c	13 633.3 \pm 0.2 ^d	32.3 \pm 5
8d	9296 \pm 8 ^c	9332.7 \pm 0.1 ^d	36.7 \pm 8
12d	2863.2 \pm 7.5 ^e	2872.2 \pm 0.1 ^d	9.0 \pm 7.5
13d	2264.0 \pm 5.0 ^e	2269 \pm 0.1 ^d	5.0 \pm 5.0
14d	1808.0 \pm 7.5 ^e	1823.0 \pm 0.1 ^d	15.0 \pm 7.5
15d	1476.1 \pm 15.0 ^e	1486.3 \pm 0.1 ^d	10.2 \pm 15.0
16d	1211.2 \pm 15.0 ^e	1227.4 \pm 0.1 ^d	16.2 \pm 15.0
17d	1005.4 \pm 15.0 ^e	1025.3 \pm 0.1 ^d	19.9 \pm 15.0

^aReference 1, anticrossing spectroscopy.

^bReference 15, anticrossing spectroscopy.

^cReference 2, anticrossing spectroscopy.

^dReference 13, microwave optical resonance spectroscopy.

^eThis work, double-resonance laser spectroscopy.

topic effects cannot cause such large shifts. The normal mass shift is given by

$$\Delta E_{\text{nms}}(^4\text{He}-^3\text{He}) = \frac{m}{M_4} E_0(^4\text{He}) - \frac{m}{M_4} \left[\frac{m + M_4}{m + M_3} \right] E_0(^4\text{He}), \quad (5)$$

where M_3 and M_4 are the masses of the ^3He and ^4He nuclei, respectively, and m is the electron mass.

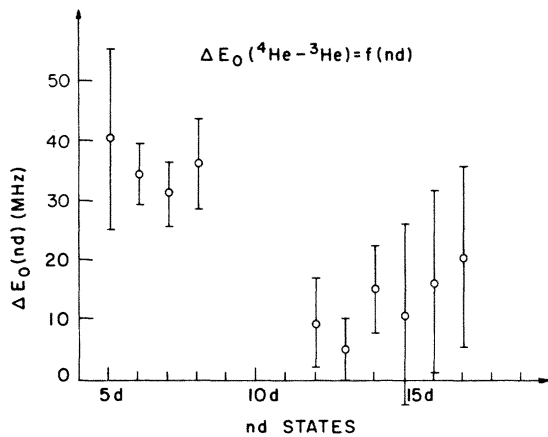


FIG. 4. Difference of the electrostatic energy intervals $\Delta E_0(nd)$ (see text for explanation) in d states between ^4He and ^3He as a function of the principal quantum number n . The data for the states $n=5-8$ obtained by anticrossing spectroscopy is taken from Refs. 1 and 2.

For the states $n=5-17$, a normal mass shift of less than 1 MHz can be calculated using Eq. (5). The specific mass shift due to the correlation of the electrons is difficult to calculate because exact wave functions for the nd states do not exist. However, one can assume that the specific mass shift should be no larger than the normal mass shift. A volume shift is negligible in helium atoms.

A possible explanation for the anomalous behavior was offered in Ref. 1. The strong hf interactions in ^3He could produce some configuration interactions which should lead to additional shifts in the $^1D-^3D$ electrostatic energy intervals. The hf interactions are similar for all nd states. Since the singlet-triplet separation decreases with higher n , one might expect the effect of configuration interaction to increase with increasing n . However, we find smaller shifts for the $n=12-17$ states than were found in the $n=5-8$ states. We feel that a satisfactory explanation for the anomalous isotopic shift has not yet been found.

V. CONCLUSION

In conclusion, we have shown that by double-resonance spectroscopy with a single-mode color center laser and the frequency-doubled output of a single-mode dye laser, precision Doppler-free measurements in Rydberg levels of ^3He can be carried out. The experimental results for the $n^{1,3}D$ hf splittings ($n=12-17$) are in excellent agreement with

semiempirical calculations using hydrogenlike wave functions. Anomalous isotopic shifts in the electrostatic energy intervals of 5–20 MHz were found for the states $n = 12$ –17. The shifts are smaller than the shifts of about 35 MHz found for the states $n = 5$ –8 with the help of anticrossing spectroscopy. No satisfactory explanation of this shift has yet been found.

ACKNOWLEDGMENTS

This work was supported by the National Science Foundation under Grant No. PHY-80-10689 and by the U.S. Office of Naval Research under Contract No. ONR N00014-78-C-0403. One of us (L.A.B.) acknowledges support by the National Science Foundation. The work of H.G. was supported by a Heisenberg Fellowship.

-
- ¹J. Derouard, M. Lombardi, and R. Jost, *J. Phys. (Paris)* **41**, 819 (1980).
- ²R. Panock, R. R. Freeman, B. R. Zegarski, and T. A. Miller, *Phys. Rev. A* **25**, 869 (1982).
- ³J. P. Descoubes, in *Physics of One- and Two-Electron Atoms*, edited by F. Bopp and H. Kleinpoppen (North-Holland, Amsterdam, 1969), p. 341.
- ⁴F. Biraben, E. Declercq, E. Giacobino, and G. Grynberg, *J. Phys. B* **13**, L685 (1980).
- ⁵T. W. Hänsch and P. Toschek, *Z. Phys.* **236**, 213 (1970).
- ⁶H. Gerhardt and T. W. Hänsch, *Opt. Commun.* **41**, 17 (1982).
- ⁷L. A. Bloomfield, H. Gerhardt, T. W. Hänsch, and S. C. Rand, *Opt. Commun.* **42**, 247 (1982).
- ⁸T. W. Hänsch and B. Couillaud, *Opt. Commun.* **35**, 441 (1980).
- ⁹T. A. Miller and R. S. Freund, *Adv. Magn. Reson.* **9**, 49 (1976).
- ¹⁰N. Bessis, H. Lefebvre-Brion, and C. M. Moser, *Phys. Rev.* **135**, A957 (1964).
- ¹¹S. D. Rosner and F. M. Pipkin, *Phys. Rev. A* **1**, 571 (1970).
- ¹²J. E. Lawler, A. I. Ferguson, J. E. M. Goldsmith, D. J. Jackson, and A. L. Schawlow, *Phys. Rev. Lett.* **42**, 1046 (1979).
- ¹³J. W. Farley, K. B. MacAdam, and W. H. Wing, *Phys. Rev. A* **20**, 1754 (1979).
- ¹⁴H. A. Schuessler, E. N. Fortson, and H. G. Dehmelt, *Phys. Rev.* **187**, 5 (1969).
- ¹⁵H. J. Beyer and K. J. Kollath, *J. Phys. B* **10**, L5 (1977).